Journal of Drug Delivery Science and Technology 88 (2023) 104981

Contents lists available at ScienceDirect

Journal of Drug Delivery Science and Technology

journal homepage: www.elsevier.com/locate/jddst

Disulfiram encapsulated in polymer nanoparticles ameliorates thioacetamide-induced liver injury

Wei Xu [a,*], Yuta Kadoya [a], Kaito Sennari [a], Waliul Islam [a], Tianli Zhang [b], Tomohiro Sawa [b], Fumika Akizuki [c], Hisaaki Hirose [d], Shiroh Futaki [d], Yukio Fujiwara [c], Yoshihiro Komohara [c], Takuro Niidome [a,**]

[a] Faculty of Advanced Science and Technology, Kumamoto University, 2-39-1 Kurokami, Chuo-ku, Kumamoto, 860-8555, Japan
[b] Department of Microbiology, Graduate School of Medical Science, Kumamoto University, 1-1-1 Honjo, Chuo-ku, Kumamoto, 860-8556, Japan
[c] Department of Cell Pathology, Graduate School of Medical Science, Kumamoto University, 1-1-1 Honjo, Chuo-ku, Kumamoto 860-8556, Japan
[d] Institute for Chemical Research, Kyoto University, Gokasho, Uji, Kyoto, 611-0011, Japan

ARTICLE INFO

Keywords:
Macrophages
Nanoparticles
Disulfiram
Anti-inflammation
Cellular uptake

ABSTRACT

Liver disease is the cause of approximately 2 million deaths per year worldwide. Liver macrophages (Kupffer cells), the most abundant immune cells in the liver, play important roles in innate immunity and contribute to many liver diseases. Disulfiram (DSF), a drug used to treat alcohol abuse, has attracted increasing attention due to its anti-cancer and anti-inflammatory effects. However, DSF accumulates in several cell types, and few studies have examined its utility as a potential treatment for liver injury. Here, we investigated the biological efficacy of DSF encapsulated in poly(lactic-co-glycolic) acid nanoparticles (DSF@PLGA NPs). *In vitro,* DSF@PLGA NPs had low cytotoxicity, were selectively taken up by the human macrophage cell line THP-1 *via* macropinocytosis, and inhibited lipopolysaccharide-induced proinflammatory cytokine production by THP-1 cells. Intravenously administered PLGA NPs predominantly localized to the liver, specifically CD68-positive Kupffer cells, and DSF@PLGA NPs significantly ameliorated thioacetamide-induced proinflammatory cytokine production and liver injury. Our results indicate that encapsulation in PLGA NPs promotes specific delivery of DSF to Kupffer cells and reduces liver injury and inflammation, suggesting that DSF@PLGA NPs may be a promising treatment for liver disease.

1. Introduction

Liver disease causes an estimated 2 million deaths annually worldwide, and the incidence is increasing [1]. As the largest organ in the human body, the liver plays critical roles in the maintenance of metabolic and immune homeostasis; accordingly, disruption of liver function leads to disorders such as alcoholic liver disease, nonalcoholic fatty liver disease, liver fibrosis, and liver cancer [2]. Liver-resident macrophages, or Kupffer cells, are non-parenchymal cells that account for 80–90% of all macrophages in the body [3]. Kupffer cells play a prominent role in acute and chronic liver diseases by virtue of their ability to produce inflammatory cytokines and chemokines [4]. Therefore, one approach to the treatment of various forms of liver injury may be to selectively inhibit the inflammatory responses of Kupffer cells.

Disulfiram (DSF) is approved by the United States Food and Drug Administration (FDA) for the treatment of alcoholism. DSF inhibits the activity of aldehyde dehydrogenase (ALDH) in the liver, which results in extreme hangover symptoms when consumed with alcohol [5]. DSF has been shown to form complexes with copper that inhibit activation of the transcription factor NF-κB in cancer cells, leading to oxidative stress [6]. DSF also reduces migration of macrophages to the tumor site by inhibiting FROUNT, a protein that regulates signaling *via* the chemokine receptors CCR2 and CCR5 [7,8]. Thus, in recent years, DSF has been the focus of many studies as a potential treatment for cancer [9]. Because DSF is FDA-approved, has a good clinical safety profile, and is inexpensive, there is interest in its off-label use to treat liver disease. One drawback, however, is that DSF lacks specificity and accumulates in many cell types, raising concern that inhibition of ALDH activity in hepatocytes and the resulting accumulation of acetaldehyde would likely increase off-target side effects such as hypotension, tachycardia,

* Corresponding author.
** Corresponding author.
E-mail addresses: xuwei@kumamoto-u.ac.jp (W. Xu), niidome@kumamoto-u.ac.jp (T. Niidome).

https://doi.org/10.1016/j.jddst.2023.104981
Received 8 March 2023; Received in revised form 10 September 2023; Accepted 20 September 2023
Available online 21 September 2023
1773-2247/

and peripheral neuropathy [10,11]. Therefore, new methods to selectively target DSF to Kupffer cells are needed to enhance the anti-inflammatory effects of DSF while reducing potential side effects.

We speculated that both of these goals could be achieved by encapsulation of DSF into polymer nanoparticles (NPs), a well-characterized method of targeting therapeutic agents to the liver, particularly Kupffer cells. Previous studies have shown that approximately 30%–99% of intravenously (i.v.) administered NPs accumulate and are sequestered in the liver [12]. Poly(lactic-co-glycolic) acid (PLGA), an FDA-approved biodegradable polymer, has high biocompatibility and has been widely used for the controlled and targeted delivery of drugs [13]. Moreover, PLGA NPs have reduced hepatotoxicity compared with silica or metal NPs, which have been reported to induce liver injury [14,15]. In general, the uptake of NPs by different cell types in the liver is controlled by the NP size [16]. NPs >200 nm in diameter tend to be taken up by Kupffer cells, and the degree of uptake correlates positively with NP size [17], whereas NPs smaller than 50 nm tend to be taken up by hepatocytes [18]. However, the toxicity of NPs also increases with size [19]; therefore, a diameter limited to about 200 nm is preferred for targeting of NPs to Kupffer cells.

In the present study, we examined the potential for encapsulation in PLGA NPs to achieve targeted delivery of DSF to macrophages and to ameliorate liver damage in a manner that was non-cytotoxic, particularly towards hepatocytes. We performed *in vitro* and *in vivo* experiments to characterize the physical and biological properties of DSF@PLGA NPs, their uptake by liver macrophages, and their anti-inflammatory effects in thioacetamide (TAA) liver injury model mice. Our results suggest that formulation of DSF in PLGA NPs may be a safe, inexpensive, and effective approach to ameliorate liver injury.

2. Materials and methods

2.1. Materials

PLGA polymer (50:50, inherent viscosity of 0.55–0.75 dL/g in chloroform, average molecular weight of 30–60 kDa) was purchased from LACTEL Absorbable Polymers (Birmingham, AL, USA). DSF, chlorpromazine hydrochloride, filipin III, and 4-methylpyrazole were purchased from Tokyo Chemical Industries (Tokyo, Japan). 1,1′-Dioctadecyl-3,3,3′,3′-tetramethylindocarbocyanine perchlorate (DiI), 1,1′-dioctadecyl-3,3,3′,3′-tetramethylindotricarbocyanine perchlorate (DiR), and 5-(N-ethyl-N-isopropyl) amiloride (EIPA) were purchased from Sigma Aldrich (St. Louis, MO, USA). All others chemicals and cell culture media were purchased from FUJIFILM Wako Pure Chemical Industries (Tokyo, Japan).

2.2. Preparation of NPs using a microfluidic system

PLGA polymer (30 mg) and DSF (9 mg) were dissolved in 5 mL of acetone. The acetone solution (organic phase) was flowed at 1.5 mL/min and water (aqueous phase) was flowed at 4.5 mL/min and mixed in a microfluidic channel (LTF-0.12.00–4256; Little Things Factory, Elsoff, Germany). The resulting solution was mixed with 2 mL of 1 wt% polyvinyl alcohol (5 kDa) as a surfactant to improve the dispersion stability of NPs. After stirring for 24 h to evaporate the acetone, large aggregates and DSF crystals were removed by centrifugation at 1000×*g* for 10 min, and NPs were collected by further centrifugation at 10,000×*g* for 10 min. DSF-free PLGA NPs were prepared in the same manner except that DSF was omitted. For flow cytometry and fluorescence microscopy, NPs were prepared by replacing DSF with 0.5 wt% of the hydrophobic fluorescent dyes DiI or DiR.

2.3. NP characterization and measurement of DSF release in vitro

The average diameter, polydispersity index, and zeta potential of NPs were measured by dynamic light scattering (DLS) method using a Malvern Zetasizer Nano ZS (Malvern Instruments, Malvern, UK) at 25 °C with a scattering angle of 173°. To evaluate the stability, the size of NPs was measured by DLS method after suspension in RPMI 1640 medium supplemented with 10% fetal bovine serum (FBS; Funakoshi, Tokyo, Japan) and incubation at 37 °C within 24 h.

The surface morphology of NPs was observed by scanning electron microscopy (SEM) at an operating voltage of 10 kV (SU8000; Hitachi High Technologies, Tokyo, Japan) and by transmission election microscopy (TEM) at an operating voltage of 80 kV (JEOL-2100F; JOEL, Tokyo, Japan). For SEM observation, NPs solution was dropped onto a glass slide and vacuum-dried at room temperature overnight. Platinum was sputtered on the samples before the observation. For TEM observation, NPs solution was dropped onto a a carbon film-coated copper mesh TEM grid (ELS-C10, Okenshoji Co., Ltd., Tokyo, Japan) for 2 min. After rinshing with water, the grid was vacuum-dried at room temperature overnight.

To determine the DSF loading and encapsulation efficiencies, samples of DSF@PLGA NPs were lyophilized using a freeze dryer (FDU-1200; EYELA, Tokyo, Japan) and dissolved in chloroform for 1 min with sonication. After evaporation of the solvent, DSF was dissolved in ethanol and quantified by HPLC with ultraviolet detection at 278 nm (Shimazu, Kyoto, Japan). The mobile phase was methanol/water (70/30) delivered at a flow rate of 1.0 mL/min through an L-Column ODS (4.6 × 15 mm, Chemicals Inspection and Testing Institute, Tokyo, Japan). To evaluate DSF release, DSF@PLGA NPs were suspended in phosphate buffered saline (PBS, pH 7.4) and incubated at 37 °C with shaking for up to 14 days. The samples were then centrifuged at 10,000×*g* for 10 min, the supernatants were collected, and the DSF concentration was quantified by HPLC as described above. Here, a standard calibration curve of DSF was measured in the concentration range of 6.25–100 μg/mL by using HPLC method. The limits of detection (LOD) and quantification (LOQ) were obtained based on the standard deviation (SD) of response and slope of calibration curve. LOD was calculated as 3 × SD/slope, and LOQ was calculated as 10 × SD/slope [20].

2.4. Cell culture

The human monocyte-like cell line THP-1 was obtained from American Type Culture Collection (Manassas, VA, USA) and cultured in RPMI 1640 medium supplemented with 10% FBS and 100 mg/mL penicillin and streptomycin (Nacalai Tesque, Kyoto, Japan) at 37 °C in a 5% CO_2 atmosphere. HepG2, a human hepatocellular carcinoma line, was obtained from Japanese Collection of Research Bioresource Cell Bank (Osaka, Japan) and cultured in DMEM (low glucose) medium supplemented with 10% FBS and 100 mg/mL penicillin and streptomycin at 37 °C in a 5% CO_2 atmosphere. To induce macrophage differentiation, THP-1 cells were treated with 100 ng/mL phorbol 12-myristate 13-acetate (PMA; Funakoshi) for 24 h. After macrophage differentiation and adhesion to the culture plates, fresh medium was exchanged and the cells were further cultured for 48 h at 37 °C.

2.5. Cell viability assay

Cytotoxicity was measured using the MTT (1-(4,5-dimethylthiazol-2-yl)-3,5-diphenylformazan; Dojindo Laboratories, Kumamoto, Japan) assay. HepG2 cells and PMA-differentiated THP-1 cells were seeded at 5 × 10^4 cells/well into 96-well plates and cultured for 24 h at 37 °C. DSF (1.9–60 μg/mL) and DSF@PLGA NPs (25–400 μg/mL) were added to the cells and the plates were incubated for an additional 24 h. Due to its hydrophobicity, DSF was dissolved in dimethyl sulfoxide (DMSO) and diluted with RPMI 1640 medium before addition to the cells. The final concentration of DMSO in culture was 0.1%. After incubation, the culture medium was removed and replaced with fresh medium containing MTT (0.5 mg/mL) for 2 h. The formazan product was then dissolved in DMSO and the absorbance at 570 nm was measured using an Infinite F50

Microplate Reader (TECAN, Mannedorf, Switzerland).

2.6. ALDH assay

ALDH activity was analyzed by measuring NADH production in a spectrophotometric assay [21]. Briefly, HepG2 cells were treated with DSF (1.9 and 3.8 μg/mL) and DSF@PLGA NPs (25 and 50 μg/mL) for 24 h, scraped into 5 mM Tris-HCl buffer (pH 7.5) containing 0.25 M sucrose, 0.5 mM ethylenediamine-tetraacetic acid (EDTA), and 0.5 mM dithiothreitol, and then centrifuged at 8000×*g* at 4 °C for 15 min. The supernatant was mixed with 0.1 mM pyrazole, 2 μM rotenone, 0.5 mM NAD^+, and 50 μM acetaldehyde, and incubated at 25 °C for 20 min. NADH was measured at 340 nm before and after incubation using a V-670 spectrophotometer (JASCO Corporation, Tokyo, Japan). Samples without acetaldehyde were used as background controls.

2.7. Measurement of cellular uptake of NPs

For the flow cytometric assay, HepG2 and PMA-differentiated THP-1 cells were placed in 12-well plates at 1×10^5 cells/well and treated with 150 μg/mL of DiI-labeled PLGA NPs for between 2 and 24 h. After incubation, the cells were washed twice with cold PBS and detached by incubation with 0.25% trypsin-EDTA at 37 °C. The cells were collected by centrifugation at 3×*g* for 5 min and resuspended in cold PBS. Data were acquired on 10,000 cells per sample, with debris and doublets excluded by gating, using a FACSCelesta instrument (BD Biosciences, San Jose, CA, USA). Data were analyzed using FlowJo software (TreeStar, Ashland, OR, USA).

For the fluorescence microscopy, HepG2 and PMA-differentiated THP-1 cells were placed in glass-bottomed dishes (35-mm diameter) at 1×10^5 cells/well and incubated with 150 μg/mL of DiI-labeled PLGA NPs for 24 h. After incubation, the cells were washed three times with PBS and fixed with 2% paraformaldehyde at 4 °C for 2 h. Nuclei were stained with 4′,6-diamidino-2-phenylindole (DAPI) for 10 min at room temperature and the cells were visualized using an Axio Observer Z1 fluorescence microscope (Carl-Zeiss AG, Oberkochen, Germany).

2.8. Determination of NP uptake pathway

To investigate the pathway by which of NPs were taken up into cells, PMA-differentiated THP-1 cells were plated at 1×10^5 cells/well and were incubated for 1 h at 37 °C with 150 μg/mL of DiI-labeled PLGA NPs in the absence (control) or presence of the following endocytic inhibitors: 5 μM cytochalasin B, 5 μM EIPA, 1 μM chlorpromazine, 2.5 μM filipin III, or 0.2% sodium azide [22,23]. At the end of the incubation, cellular uptake of NPs was evaluated and quantified using the flow cytometry and fluorescence microscopy assays described above.

For SEM, PMA-differentiated THP-1 cells were cultured on cover glasses in a 6-well plate at 1×10^5 cells/well and left untreated or incubated with PLGA NPs in the absence or presence of 5 μM EIPA at 37 °C for 1 h. The cells were washed three times with PBS, fixed with 0.1% cacodylate buffer containing 2% paraformaldehyde and 2.5% glutaraldehyde at room temperature for 30 min, and then kept at 4 °C overnight. The next day, the cells were dehydrated with a gradient of ethanol/water mixtures (20, 50, 70, 90, and 100%) for 10 min each, and then immersed in *t*-butyl alcohol and placed at −20 °C for 30 min. Frozen samples were dehydrated using an FDU-1200 freeze dryer (EYELA, Tokyo, Japan) for 24 h. The samples were then observed with an SEM (SU8000, Hitachi High Technologies, Tokyo, Japan).

2.9. In vitro cytokine production and enzyme-linked immunosorbent assay (ELISA)

THP-1 cells were placed in 12-well plates at 2×10^5 cells/well and differentiated with PMA. The cells were washed twice with PBS, and then incubated alone (control), with 3.8 μg/mL of DSF, or with 50 μg/mL of DSF@PLGA NPs (3.8 μg/mL DSF) with or without 200 ng/mL lipopolysaccharide (LPS) for 24 h. After incubation, the supernatants were harvested and concentrations of tumor necrosis factor-α (TNF-α) and interleukin-6 (IL-6) were assayed using ELISA kits (Thermo Fisher Scientific, Waltham, MA, USA) according to the manufacturer's protocol.

2.10. TAA-induced liver injury model and NP biodistribution

Animal experiments were approved by the Ethics Committee for Animal Experiments of Kumamoto University (decision number is A2021-132) and carried out according to the Laboratory Protocol of Animal Handing, Kumamoto University, Kumamoto, Japan. In addition, the animal experiments in this research work complied with the ARRIVE guidelines and were conducted as per the U.K. Animals (Scientific Procedures) Act, 1986, and associated guidelines. Male C57BL/6 mice (4 weeks of age) were purchased from SLC (Shizuoka, Japan) and maintained under conditions of controlled humidity (55%) and temperature (22 °C) with a 12 h light/dark cycle. When the mice were 6 weeks of age (18–21 g body weight), they were injected intraperitoneally (i.p.) with 90 mg/kg thioacetamide (TAA) in saline solution twice weekly for 2 weeks (4 injections).

To evaluate the biodistribution of NPs, mice were treated with TAA to induce liver injury exactly as described above. On day 16, mice were injected intravenously (i.v.) with 50 mg/kg DiR-labeled PLGA NPs and euthanized 24 h later. The kidneys, heart, liver, lungs, and spleen were collected and visualized using an IVIS Lumina Imaging system (Xenogen, Alameda, CA, USA). For quantitation, DiR was extracted as previously described [24]. Briefly, the tissues were cut into small pieces of 100 mg and homogenized in 2 mL of chloroform on ice using a Polytron tissue homogenizer (PT1200E, Kinematica AG, Lucerne, Switzerland). The samples were centrifuged at 10,000×*g* for 20 min and the supernatants containing DiR were collected, the solvent was evaporated, and the residue was redissolved in 500 μL of chloroform. Fluorescence intensity was measured at excitation/emission wavelengths of 740 nm/780 nm using a FP-6600 fluorescence spectrophotometer (Jasco Corporation).

To evaluate the anti-inflammatory effects of NPs in the TAA liver injury model, mice were treated with TAA for 2 weeks, as described above. On days 16 and 19, mice were injected i.p. with 3.8 mg/kg of free DSF or i.v. with 50 mg/kg of DSF@PLGA NPs (3.8 mg/kg DSF) and 24 h later, the mice were sacrificed. Blood samples were collected, and serum samples were prepared. TNF-α and IL-6 levels were measured using ELISA kits as described above, and aspartate aminotransferase (ALT) and alanine aminotransferase (AST) levels were measured using a Transaminase C Test Kit (Wako Pure Chemical Industries).

For histopathological analysis, the liver tissues were fixed in formalin for 24 h, dehydrated in graded alcohol and embedded in paraffin blocks. The liver sections were prepared at 3 μm thickness and subjected to hematoxylin and eosin (H&E) staining.

2.11. Statistical analysis

Experiments were performed in triplicate and data are presented as the mean ± standard error (SEM). Data were analyzed using Student's t-test and analysis of variance (ANOVA), followed by the Bonferroni post hoc adjustment for multiple comparisons. A difference was considered to be statistically significant when the p value was <0.05.

3. Results and discussion

3.1. NP characterization and release of DSF in vitro

DSF-free PLGA NPs and DSF@PLGA NPs were fabricated using a microfluidic device. The average diameter, polydispersity index (PDI), and zeta potential of the NPs were analyzed by dynamic light scattering

Table 1
Characterization, drug loading and encapsulation efficiency of NPs.

NP formulation	Diameter (nm)	PDI	Zeta potential (mV)	Drug load (%)	Encapsulation efficiency (%)
PLGA	241.3 ± 4.8	0.059 ± 0.005	−27.3 ± 3.1	N/A	N/A
DSF@PLGA	230.3 ± 5.3	0.14 ± 0.038	−26.4 ± 3.3	7.4 ± 0.13	43.4 ± 1.3

Data represent the mean ± standard deviation of triplicates. DSF: disulfiram, N/A: not applicable, NP: nanoparticle, PDI: polydispersity index, PLGA: poly(lactic-co-glycolic) acid.

(Table 1). The average diameter of the PLGA NPs was ~240 nm with a narrow size distribution (PDI <0.1), which can be attributed to the advantage of the microfluidic system. The zeta potential of PLGA NPs was −27 mV, suggesting that the NPs would have a lower tendency to absorb proteins than positively charged NPs [25]. The surface charge of NPs is known to be an important factor for cellular uptake behavior, and macrophages are more likely to take up negatively charged NPs compared with positively charged NPs [26–28]. The characteristics of DSF@PLGA NPs were similar to those of the PLGA NPs (Table 1 and Fig. 1). Although the PDI of DSF@PLGA NPs was higher than that of PLGA NPs (~0.14 *vs* ~0.06), SEM and TEM imaging demonstrated that DSF@PLGA NPs were uniform in size (Fig. 1C). Furthermore, the particle size of DSF@PLGA NPs was shown to be stable after incubation in RPMI 1640/10% FBS medium at 37 °C for 24 h (Fig. 1D).

According to the standard calibration curve of DSF (Fig. S1; linearity $R^2 > 0.99$), DSF loading and encapsulation efficiency in PLGA NPs were calculated to be 7.4% and 43.4%, respectively (Table 1), which are similar to or slightly higher than the corresponding values reported by others who investigated the anti-cancer activity of DSF@PLGA NPs using cancer cell lines [29,30]. In addition, the limit of detection (LOD) of DSF was 0.013 μg/mL and the limit of quantification (LOQ) of DSF was 0.039 μg/mL. The release kinetic of DSF@PLGA NPs in PBS (pH 7.4) or PBS containing 10% FBS at 37 °C for up to 7 days was quantified (Fig. 1E). In PBS, approximately 24% DSF was released in the first 24 h followed by release of up to ~70% DSF within 7 days. Whereas, in PBS containing 10% FBS, silimar ~24% DSF was released in the first 24 h but followed by a higher release rate of up to 100% DSF within 3 days. The

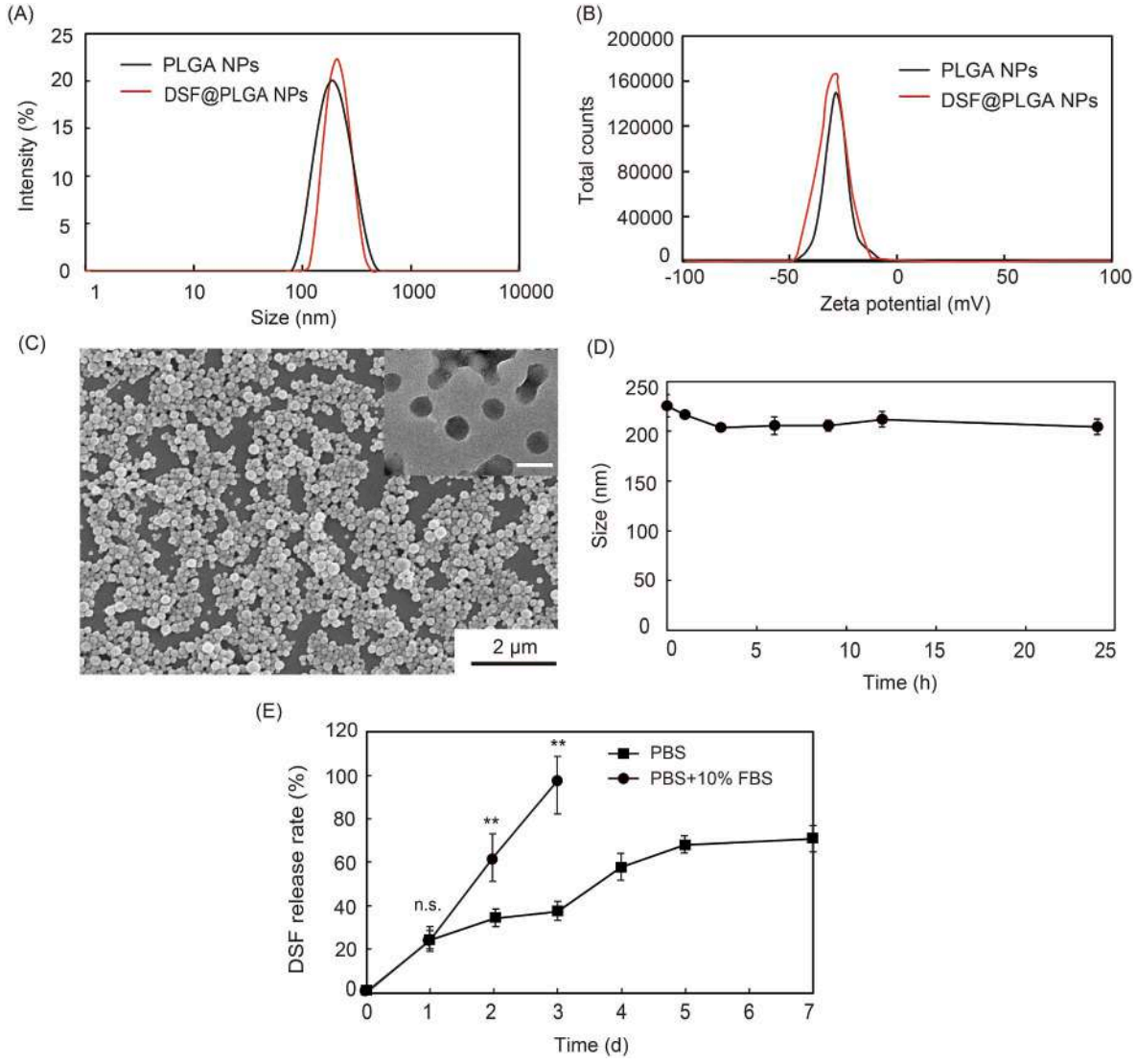

Fig. 1. Characterization of PLGA NPs. (A and B) Hydrodynamic diameter (A) and (B) zeta potential of PLGA NPs and DSF@PLGA NPs. (C) SEM (scale bar = 2 μm) and TEM (inset: scale bar = 300 nm) images of DSF@PLGA NPs. (D) Stability of DSF@PLGA NPs incubated in RPMI 1640/10% FBS medium at 37 °C for up to 24 h. (E) DSF release from DSF@PLGA NPs incubated in PBS (pH 7.4) or PBS containing 10% FBS at 37 °C for up to 7 days. Data represent the mean ± SEM of triplicates. $^{**}p < 0.01$; n.s., not significant for differences between PBS and PBS containing 10% FBS.

accelerated DSF release from NPs was probably due to the serum in PBS which improved the solubility of DSF. This is a common phenomenon observed in release kinetics study of poorly water-soluble drugs [31].

3.2. Cytotoxicity of NPs

To evaluate the potential cytotoxicity of PLGA NPs and DSF@PLGA NPs for liver macrophages *vs* hepatocytes, we used the human monocyte-like cell line THP-1 and the human hepatoblastoma cell line HepG2 cells. THP-1 cells were induced to differentiate into macrophages by treatment with PMA for 24 h HepG2 or differentiated THP-1 cells were then incubated with 25–400 μg/mL of DSF@PLGA NPs (1.9–60 μg/mL DSF) or free DSF at 1.9–60 μg/mL for 24 h and cell viability was measured using the MTT assay. Free DSF exhibited relatively little cytotoxicity towards THP-1 cells compared with HepG2 cells (Fig. 2). Thus, at the highest concentration of free DSF tested, 60 μg/mL (~200 μM), HepG2 cell viability was reduced to 5%–10% whereas THP-1 cell viability remained high at 67%. This result is consistent with a previous demonstration that free DSF is more toxic to HepG2 cells than to the human embryonic kidney cell line HEK-293 [32]. Notably, encapsulation of DSF into PLGA NPs reduced the cytotoxicity of DSF for both cell lines (Fig. 2), which was likely a result of the slow release of NP-encapsulated DFS, as shown above, and reduced exposure to the cells. DSF-free PLGA NPs at concentrations up 800 μg/mL were not cytotoxic to HepG2 or THP-1 cells (cell viability >80%; Fig. S2). Based on these results, we selected the non-toxic concentrations of 3.8 μg/mL free DSF and 50 μg/mL DSF@PLGA NPs (3.8 μg/mL DSF) for further experiments.

3.3. ALDH activity in HepG2 cells

We determined the effect of DSF@PLGA NPs on ALDH activity in HepG2 cells, which have been reported to behave similarly to normal human hepatocytes in terms of ALDH regulation [33]. HepG2 cells were incubated alone (control), with free DSF at 1.9 and 3.8 μg/mL, or with DSF@PLGA NPs at 25 and 50 μg/mL (1.9 and 3.8 μg/mL DSF) for 24 h and ALDH activity was then measured. Free DSF at 1.9 μg/mL had no effect on ALDH activity, whereas the activity was decreased by ~50% at 3.8 μg/mL. However, encapsulation of DSF prevented ALDH inhibition, as demonstrated by the lack of significant effect of DSF@PLGA NPs on ALDH activity at either DSF concentration (Fig. 3). DSF has been reported to inhibit ALDH activity *via* formation of mixed disulfide and covalent adducts (two carbamoyl derivatives) of DSF and its metabolites with cysteine-302 at the ALDH active site [34]. These data suggest that encapsulation of DSF within PLGA NPs prevents DSF–ALDH adduct formation and inhibition of ALDH activity in hepatocytes. We also investigated the ALDH activity in THP-1 cells using the same method. However, ALDH activity in THP-1 cells was undetectable. This is consistent with the idea that ALDH is highly expressed in hepatocytes, but not in Kupffer cells [35].

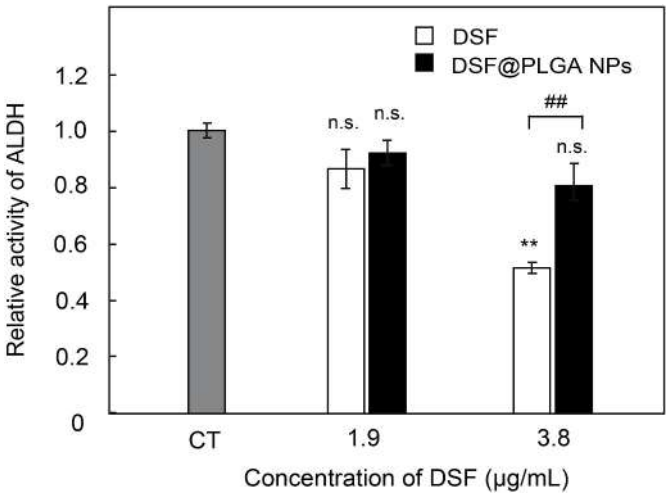

Fig. 3. Effects of free DSF and DSF@PLGA NPs on ALDH activity in HepG2 cells. Cells were incubated in the absence (CT) or presence of free DSF or DSF@PLGA NPs at 37 °C for 24 h. Data are presented as the mean ± SEM of triplicates. $^{**}p < 0.01$; n.s., not significant for differences *vs* control and $\#\#p < 0.01$ for differences between DSF and DSF@PLGA NPs.

3.4. Uptake of PLGA NPs by THP-1 and HepG2 cells

To examine cellular uptake, HepG2 and differentiated THP-1 cells were incubated at 37 °C for 24 h with PLGA NPs labeled with the dye DiI, which emits fluorescence at ~570 nm and can thus be detected in the phycoerythrin (PE) channel of flow cytometers. As shown in Fig. 4A, PLGA NPs were taken up much more rapidly and extensively by THP-1 compared with HepG2 cells. Essentially 100% of THP-1 cells had taken up DiI-PLGA NPs by 16–24 h, compared with only about 20% of HepG2 cells over the same incubation time (Fig. 4A and B). We also analyzed the cells by fluorescence microscopy, which confirmed the marked accumulation of NPs in differentiated THP-1 cells compared with HepG2 cells (Fig. 4C).

The preferential uptake of PLGA NPs by THP-1 cells could be related to the physicochemical properties of the NPs, such as size, shape, and

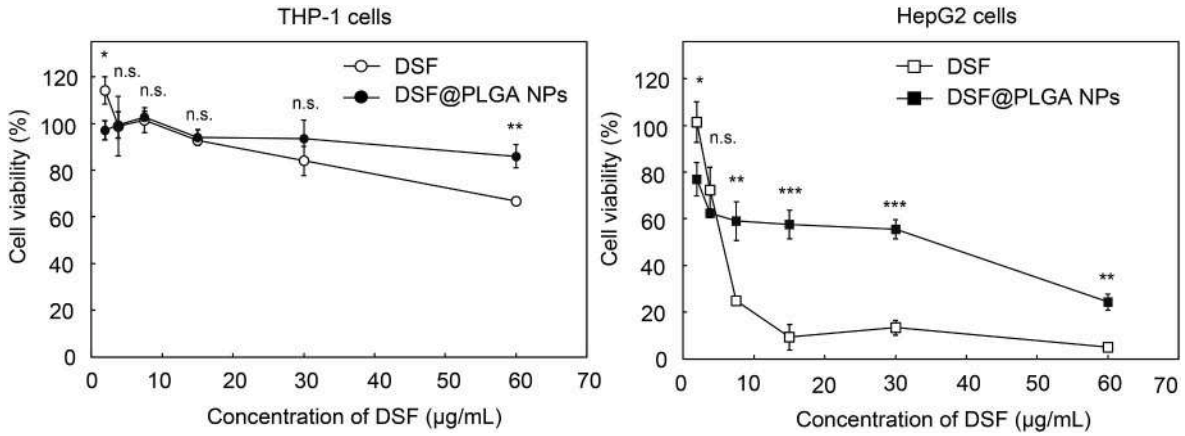

Fig. 2. Cytotoxicity of DSF and DSF@PLGA NPs. Viability of (A) THP-1 cells and (B) HepG2 cells was evaluated using the MTT assay after incubation with the indicated concentration of free DSF or DSF@PLGA NPs at 37 °C for 24 h. Data are presented as the mean ± SEM of triplicates. $^{*}p < 0.05$, $^{**}p < 0.01$, $^{***}p < 0.001$; n.s., not significant for differences between DSF and DSF@PLGA NPs.

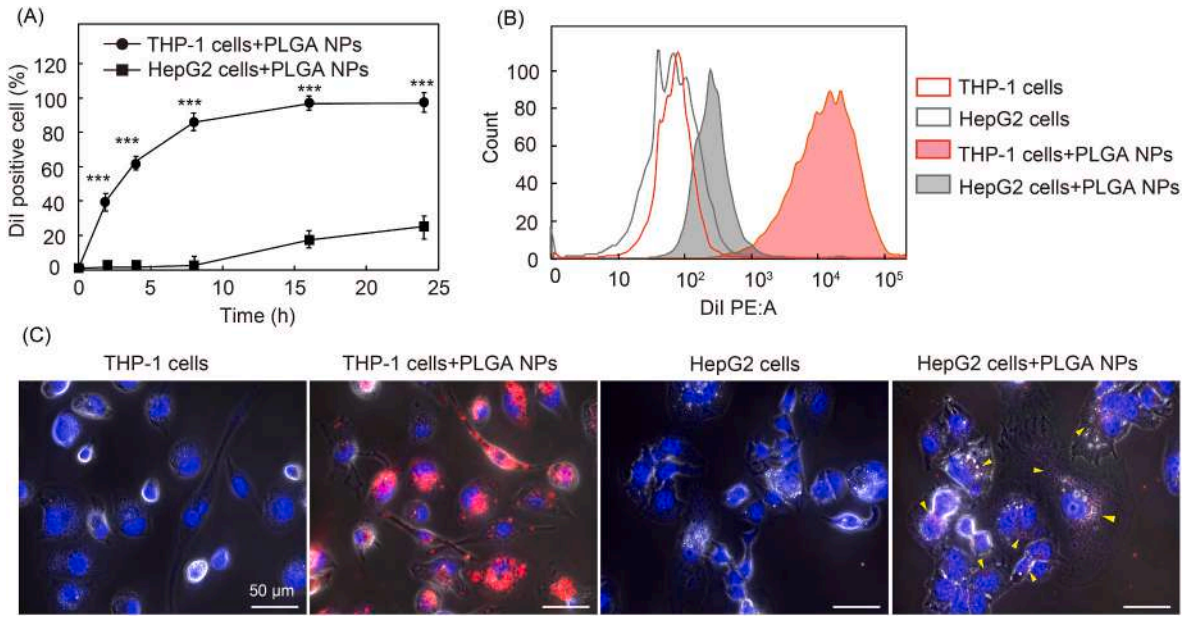

Fig. 4. Cellular uptake of DiI-labeled PLGA NPs by THP-1 and HepG2 cells. (A) Time course of DiI-labeled PLGA NP uptake by THP-1 and HepG2 cells measured by flow cytometry after incubation at 37 °C for up to 24 h. (B) Representative flow cytometry histograms of the cells incubated at 37 °C for 24 h as in (A). (C) Fluorescence microscopy images of DiI-labeled PLGA NP uptake (red) by THP-1 and HepG2 cells after incubation at 37 °C for 24 h. Nuclei were stained with DAPI (blue). Yellow arrows indicate DiI-labeled PLGA NPs uptake by HepG2 cells. Scale bar = 50 μm. Data are presented as the mean ± SEM of triplicates. ***$p < 0.001$ for differences between THP-1 cells and HepG2 cells. (For interpretation of the references to color in this figure legend, the reader is referred to the Web version of this article.)

zeta potential [36]. As noted, NPs >200 nm tend to be taken up by macrophages, whereas smaller sized NPs (<100 nm) are taken up not only by macrophages but also other cell types, including the liver, ovarian, and lung cancer cell lines HepG2, HeLa, and A549, respectively [37–39]. We also evaluated cellular uptake of NPs by the murine macrophage cell line RAW 264.7. Incubation of cells with 100 μg/mL DiI-PLGA NPs at 37 °C for 24 h resulted in uptake by 39% of RAW 264.7 cells, 46% of undifferentiated THP-1 cells, and 64% of PMA-differentiated THP-1 cells (Fig. S3). This is consistent with the effects of PMA treatment which increases the endocytosis activity of THP-1 cells [40].

3.5. Identification of the pathway of PLGA NP uptake by THP-1 cells

To determine the mechanism by which DiI-PLGA NPs were taken up by differentiated THP-1 cells, we incubated the cells for 1 h at 37 °C with optimal non-toxic concentrations of several endocytosis inhibitors; namely, sodium azide (NaN3), cytochalasin B (CytB), EIPA, chlorpromazine (Chlor), and filipin III [22,23]. These agents inhibit (i) energy-dependent endocytosis (NaN3); (ii) phagocytosis, an actin-dependent pathway preferentially used by "professional phagocytes" to engulf large particles such as bacteria and cell debris (CytB) [41]; (iii) macropinocytosis, an actin-dependent nonspecific endocytic pathway mediated by the formation of large membrane protrusions (EIPA) [42]; (iv) clathrin-dependent endocytosis, which involves encapsulation of transmembrane receptors and transporters (Chlor) [43]; and (v) caveolae-dependent endocytosis, which occurs *via* formation of flask-shaped membrane invaginations about 50–100 nm in diameter (filipin III) [44].

As shown in Fig. 5A and B, DiI-PLGA NP uptake by THP-1 cells was significantly inhibited by NaN3 (~80% inhibition), CytB (~20%), and EIPA (~50%), whereas Chlor and filipin showed little effect on uptake (~10% and 8%, respectively). These results suggested that PLGA NPs are taken up by THP-1 cells mainly *via* macropinocytosis and, to a lesser extent, *via* phagocytosis. This result is in agreement with a previous study suggesting that NPs of 100–200 nm diameter enter cells *via* clathrin- or caveolae-mediated endocytosis pathways, whereas those >200 nm diameter are predominantly taken up *via* phagocytosis or macropinocytosis [45]. To confirm our finding, we also examined the cells by fluorescence microscopy. In agreement with the flow cytometry assay, very few DiI-PLGA NPs were visible within EIPA-treated THP-1 cells compared with control untreated cells (Fig. 5C).

Macropinocytosis occurs through a pathway involving actin reorganization, formation of membrane protrusions (ruffling), and uptake of extracellular fluid and its contents [42]. To examine this process in more detail, we performed SEM of THP-1 cells after incubation with PLGA NPs in the absence or presence of EIPA, as previously reported [46]. We observed active membrane ruffling on the surface of THP-1 cells and PLGA NPs were localized at the sites of ruffles (Fig. 5D). However, incubation with EIPA significantly inhibited membrane ruffling, consistent with the observed reduction in cellular uptake of NPs. To determine whether uptake of PLGA NPs interfered with macropinocytosis of other molecules, we incubated THP-1 cells with rhodamine-labeled dextran (70 kDa), a common fluorescent marker of macropinocytosis [47]. Notably, we observed no difference between rhodamine-dextran uptake in the presence or absence of PLGA NPs, indicating that PLGA NPs did not interfere with macropinocytosis of other molecules (Fig. S4).

3.6. In vitro anti-inflammatory effects of DSF and DSF@PLGA NPs

We next evaluated the potential anti-inflammatory effects of DSF@PLGA NPs compared with free DSF. Differentiated THP-1 cells were untreated or stimulated with LPS in the absence or presence of free DSF (3.8 μg/mL) or DSF@PLGA NPs (50 μg/mL) for 24 h. Production of the proinflammatory cytokines TNF-α and IL-6 was then quantified by ELISA. As expected, incubation with LPS increased the production of both cytokines compared with untreated cells, but the increase was significantly attenuated by the presence of free DSF or DSF@PLGA NPs, although encapsulated DSF was much more effective (Fig. 6). Many studies have demonstrated the ability of DSF to inhibit inflammatory responses *via* effects on several mechanisms, including inhibition of the chemokine signal regulator FROUNT, the pore-forming proteins

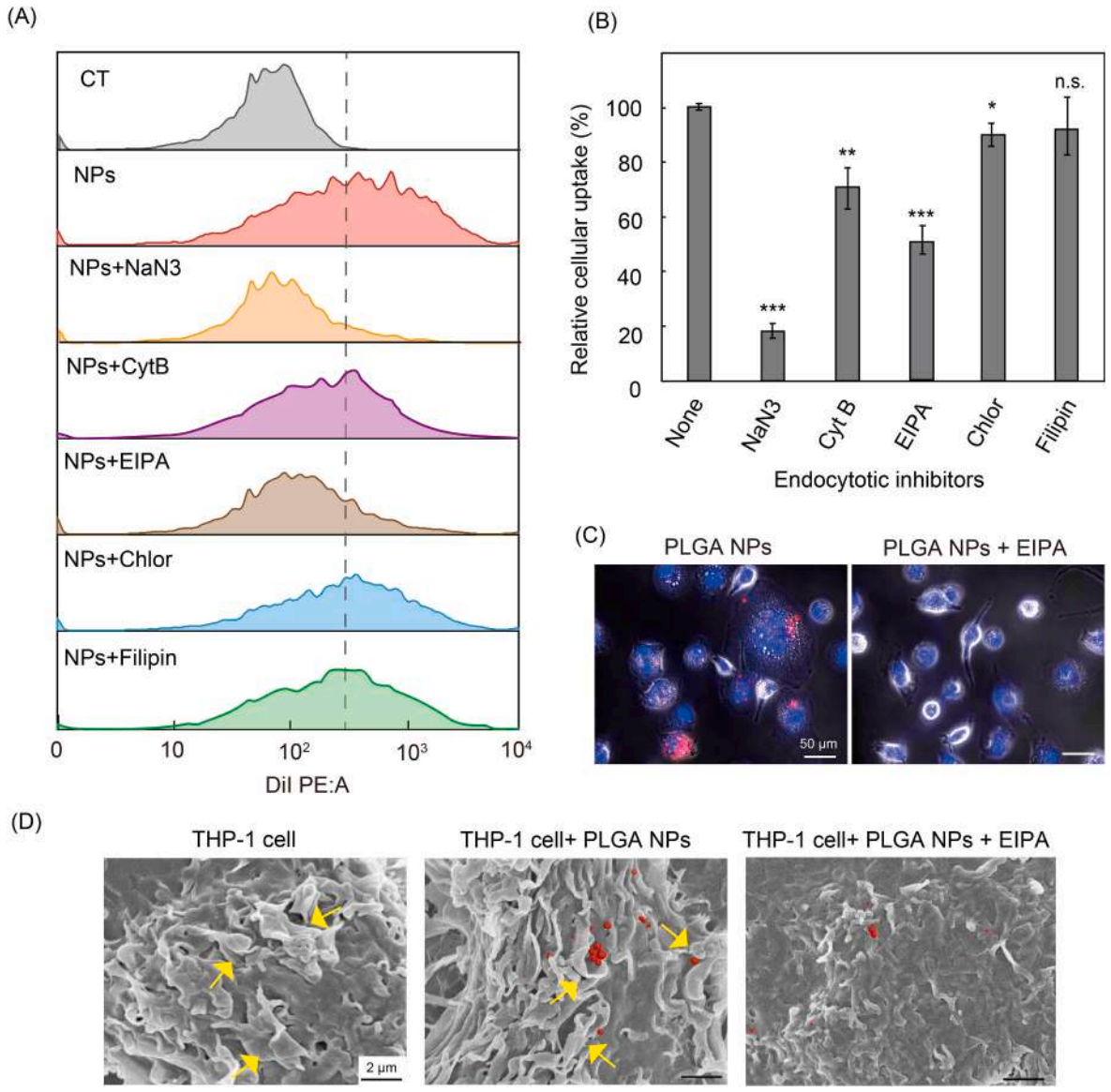

Fig. 5. Mechanism of DiI-labeled PLGA NP uptake by THP-1 cells. (A) Representative flow cytometry histograms of DiI fluorescence and (B) quantification of the relative uptake of DiI-labeled PLGA NPs after incubation of THP-1 cells for 1 h at 37 °C with sodium azide (NaN3), cytochalasin B (CytB), 5-(N-ethyl-N-isopropyl) amiloride (EIPA), chlorpromazine (Chlor), or filipin III. (C) Fluorescence microscopy images of DiI-labeled PLGA NP (red) uptake by THP-1 cells without and with EIPA treatment for 1 h. Nuclei were labeled with DAPI (blue). Scale bars = 50 μm. (D) SEM images of untreated THP-1 cells and THP-1 cells incubated with PLGA NPs in the absence or presence of EIPA for 1 h at 37 °C. NPs are pseudocolored red and membrane protrusions (ruffles) are indicated with yellow arrows. Scale bars = 2 μm. Data are presented as the mean ± SEM of triplicates. *$p < 0.05$, **$p < 0.01$, ***$p < 0.001$; n.s., not significant. (For interpretation of the references to color in this figure legend, the reader is referred to the Web version of this article.)

gasdermin D, the NF-κB pathway, and inflammasome components such as nod-like receptor protein 3 [9,48,49]. However, to the best of our knowledge, this is the first report of the ability of DSF encapsulated in NPs to directly target the macrophage inflammatory response. Thus, encapsulation in PLGA NPs may be an effective method to improve the anti-inflammatory effects of DSF.

3.7. *In vivo* distribution of PLGA NPs

Before assessing the *in vivo* efficacy of DSF@PLGA NPs for the treatment of liver injury, we analyzed the biodistribution of PLGA NPs in untreated C57BL/6 mice by injecting them i.v. with PLGA NPs labeled with the near-infrared fluorescent dye DiR, which enables 2- and 3-dimensional visualization of tissue uptake using an IVIS system. At 24 h after injection, imaging of the excised kidneys, heart, liver, lungs, and spleen showed that PLGA NPs mainly accumulated in the liver and, to a lesser extent, in the spleen, whereas no signal was detected in the kidneys, heart, or lung (Normal + PLGA NPs, Fig. 7A). Quantitative analysis of extracted organs confirmed that ~30% of injected DiR-PLGA NPs accumulated in the liver (Fig. 7B), which is consistent with the known accumulation of NPs >200 nm in Kupffer cells within the liver [50,51]. PLGA is biodegradable polymer that is degraded to lactic acid and glycolic acid, which are non-toxic and easily metabolized via Krebs cycle pathway [52]. Therefore, there is minimal toxicity associated with using PLGA NPs in drug delivery applications.

We next analyzed the distribution of DiR-PLGA NPs in C57BL/6 mice treated for 2 weeks with twice-weekly i.p. injections of TAA, a hepatotoxic compound that induces oxidative stress and inflammation in the liver *via* activation of the JNK signaling pathway [53]. Injected NPs were also found to accumulate predominantly in the livers of TAA-treated mice, but the proportion of injected NPs in the liver was significantly higher than that seen in untreated mice (~40% *vs* 30%; Fig. 7A and B).

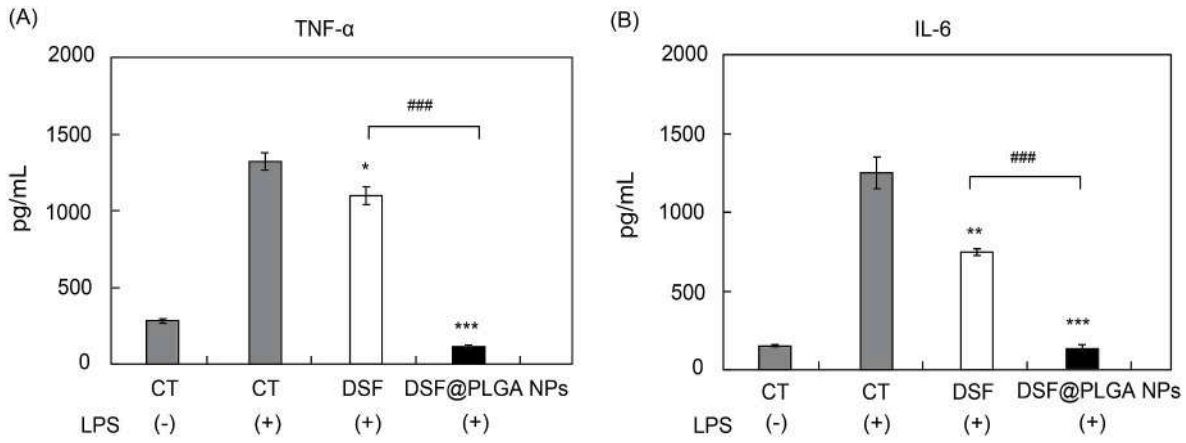

Fig. 6. Effect of free DSF and DSF@PLGA NPs on proinflammatory cytokine production by THP-1 cells. (A) TNF-α and (B) IL-6 levels produced by LPS-activated THP-1 cells incubated with or without free DSF and DSF@PLGA NPs (3.8 μg/mL equivalent) for 24 h. Data are presented as the mean ± SEM of triplicates. $*p < 0.05$, $**p < 0.01$, $***p < 0.001$ for differences *vs* control (CT+) and $###p < 0.001$ for differences between DSF (+) and DSF@PLGA NPs (+).

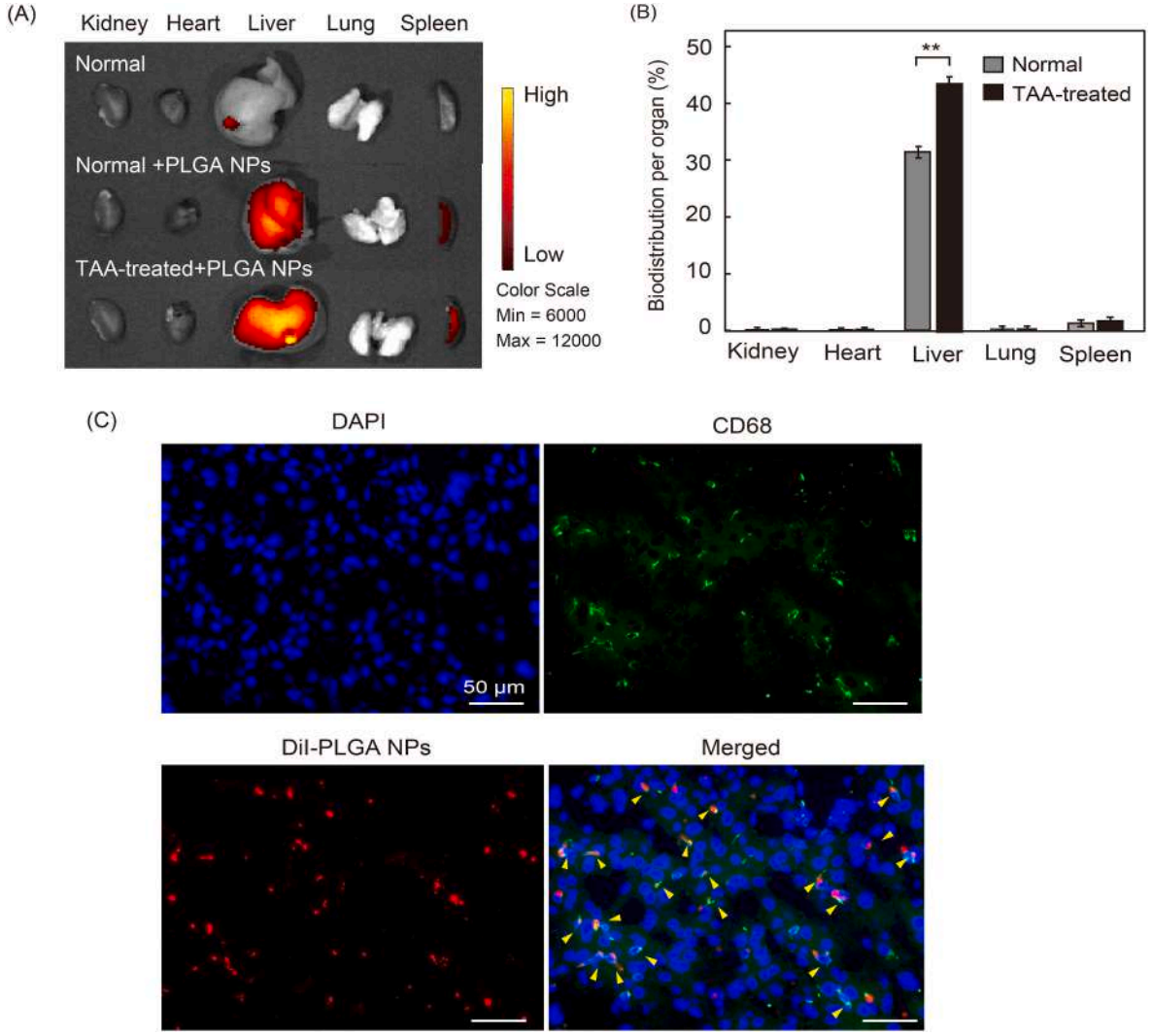

Fig. 7. Distribution of DiR-labeled PLGA NPs to the major organs of mice. Organs were harvested at 24 h after intravenous injection of NPs to untreated and thioacetamide (TAA)-treated C57BL/6 mice. (A) IVIS images and (B) quantitative analysis of DiR extracted from organs. (C) Fluorescence microscopy images of liver sections from injected mice stained with anti-CD68. Nuclei were stained with DAPI (blue). Yellow arrows indicate DiI-PLGA NPs (red) co-localized with $CD68^{+}$ (green) Kupffer cells. Data are presented as the mean ± SEM of triplicates. $**p < 0.01$. (For interpretation of the references to color in this figure legend, the reader is referred to the Web version of this article.)

This result may be due to the activation of liver-resident liver macrophages by TAA, which would lead to an increase in NP uptake [54]. Fluorescence microscopy of liver sections immunostained with an antibody against the macrophage marker CD68 [55] showed co-localization of the administered DiR-labeled PLGA NPs with $CD68^{+}$ Kupffer cells, and not with hepatocytes (Fig. 7C). This result is in agreement with previous studies of NP uptake in the liver, which demonstrated that PLGA NPs (~270 nm in diameter) mainly localized with Kupffer cells, followed by endothelial cells, hepatic stellate cells, and, to a minor degree, hepatocytes [50].

3.8. Amelioration of TAA-induced liver injury by administration of DSF and DSF@PLGA NPs

The effect of free DSF and DSF@PLGA NPs on TAA-induced liver injury in mice was evaluated by treating the mice with TAA for 2 weeks, as described above, followed by i.p. injection of 3.8 mg/kg free DSF or i.v. injection of 50 mg/kg DSF@PLGA NPs on days 16 and 19 (Fig. 8A). The administration routes of free DSF (i.p.) and DSF@PLGA NPs (i.v.) were different. Several studies conducted in the last few years reported that DSF had anti-cancer and anti-inflammatory effects [56,57]. Most of these studies used oral administration or i.p. injection rather than i.v. injection due to the low water solubility of DSF. For the administration of DSF@PLGA NPs, however, we chose i.v. rather than i.p. injection because it reportedly leads to superior accumulation of PLGA NPs in the liver [58].

Blood samples were collected 24 h later, AST and ALT levels or TNF-α and IL-6 levels were measured. As expected, AST and ALT levels were significantly increased in TAA-injected mice compared with control mice, confirming the successful induction of liver injury (Fig. 8B and C). However, administration of either free DSF or DSF@PLGA NPs significantly suppressed the TAA-induced increase in both AST and ALT, and DSF@PLGA NPs were significantly more effective than the same concentration of free DSF (Fig. 8B and C). Similar results were seen when TNF-α and IL-6 levels were measured, which also demonstrated not only the efficacy of DFS in suppressing TAA-induced inflammation but also the significantly superior efficacy of DSF@PLGA NPs compared with free DSF (Fig. 8D and E). To demonstrate the pharmacokinetics of DSF@PLGA NPs and free DSF in the liver, liquid chromatography-electrospray ionization-mass spectrometry (LC-MS) with an Agilent Ultivo Triple Quadrupole LC-MS system (Agilent Technologies, Santa Clara, CA, USA) was used (Fig. S5). Using this LC-MS system, we were

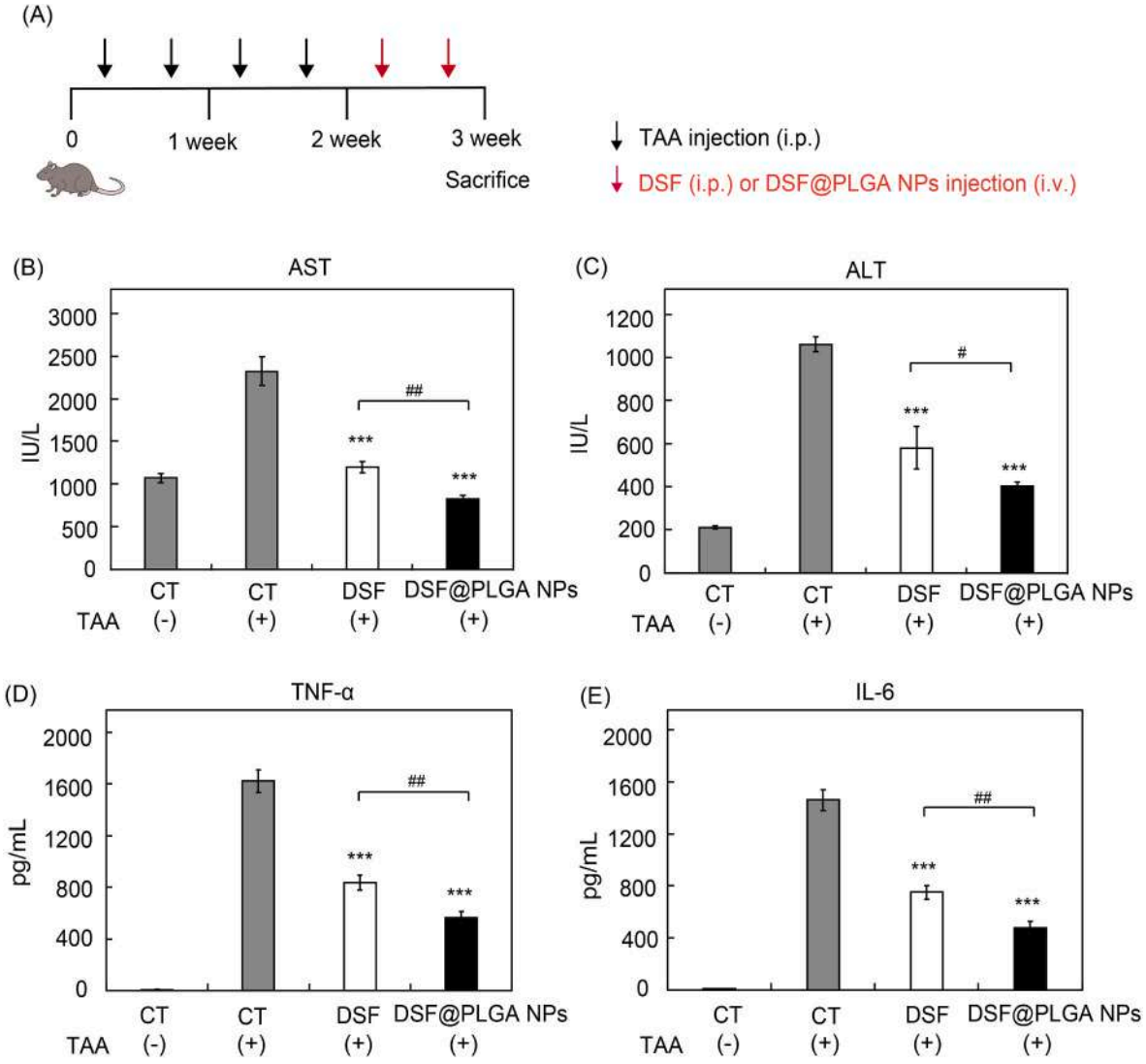

Fig. 8. Effect of free DSF and DSF@PLGA NP administration on TAA-induced hepatotoxicity. (A) Experimental protocol: TAA was injected on days 2, 5, 9, and 12, and free DSF (3.8 mg/kg i.p.) or DSF@PLGA NPs (50 mg/kg i.v.) were injected on days 16 and 19. (B–E) Aspartate aminotransferase (AST), alanine transaminase (ALT), TNF-α, and IL-6 level measured 24 h after injection of DSF and DSF@PLGA NPs. Data are presented as the mean ± SEM of triplicates. $***p < 0.001$ for differences *vs* control (CT+); $\#p < 0.05$ and $\#\#p < 0.01$ for differences between DSF (+) and DSF@PLGA NPs (+).

able to separate and identify standard samples of DSF, and confirmed that 2.5 pmol DSF was the lower limit of detection. However, due to the rapid metabolism of DSF in plasma and liver (half-life: 2–4 min) [59], free DSF in the liver was undetectable. DSF derived from DSF@PLGA NPs was also undetectable. Swider et al. reported that PLGA NPs accumulated in the liver but were rapidly degraded within 24 h, in contrast to the 72-h degradation of PLGA NPs observed in an *in vitro* experimental setting [60]. Therefore, the extinction of DSF in the liver in our experiments is probably attributable to the rapid degradation of PLGA NPs in the liver, and the immediate metabolism of released DSF.

These results are consistent with other studies indicating that free DSF reduces liver injury in carbon tetrachloride-treated mice, an effect mediated by reductions in the activation and viability of hepatic stellate cells [61]. Our results suggest that encapsulation in PLGA NPs enables the preferential delivery of DSF to Kupffer cells, thereby avoiding undesirable effects on hepatocytes and hepatic stellate cells [62,63]. To evaluate the liver damage, histopathological evaluation by hematoxylin and eosin staining of liver sections was performed (Fig. S6). We found a mild inflammatory cell infiltration in the liver tissue of TAA-treated mice, but no inflammatory tissue was observed in DSF@PLGA NPs treated mice. Collectively, DSF@PLGA NPs may therefore represent a promising therapeutic formulation for the treatment of liver injury.

4. Conclusions

In this study, we demonstrated the superior biological efficacy of DSF when encapsulated in PLGA NPs compared with free DSF. DSF@PLGA NPs exhibited reduced cytotoxicity, reduced inhibition of ALDH activity, and enhanced anti-inflammatory effects compared with free DSF. Moreover, DSF@PLGA NPs exhibited marked selectivity for uptake by macrophages compared with hepatocytes. PLGA NPs were taken up by macrophages mainly through macropinocytosis. In a mouse model of liver injury, we showed that PLGA NPs were preferentially delivered to the liver and co-localized with CD68-positive Kupffer cells. DSF@PLGA NPs also effectively ameliorated liver injury and reduced the production of proinflammatory cytokines in TAA-treated mice. Taken together, our results provide strong support for the potential utility of DSF@PLGA NPs for the treatment of liver injury.

Funding

This work was supported by grants from the Core Research for Evolutionary Science and Technology (CREST, Japan Science and Technology Agency (JST) awarded to T.N. (JPMJCR18H5).

CRediT authorship contribution statement

Wei Xu: Conceptualization, Methodology, Investigation, Writing – original draft. **Yuta Kadoya:** Data curation, Investigation. **Kaito Sennari:** Methodology, Formal analysis. **Waliul Islam:** Methodology. **Tianli Zhang:** Formal analysis. **Tomohiro Sawa:** Formal analysis. **Fumika Akizuki:** Formal analysis. **Hisaaki Hirose:** Methodology, Writing – review & editing. **Shiroh Futaki:** Methodology, Writing – review & editing. **Yukio Fujiwara:** Methodology, Writing – review & editing. **Yoshihiro Komohara:** Conceptualization, Methodology, Writing – review & editing. **Takuro Niidome:** Supervision, Conceptualization, Project administration, Writing – review & editing.

Declaration of competing interest

The authors declare no conflicts of interest.

Data availability

No data was used for the research described in the article.

Acknowledgments

We are grateful to Prof. Yoshiki Katayama and Ms. Aulia Fadlina of Kyushu University for support with the IVIS experiments. We thank Anne M. O'Rourke, PhD and Michelle Kahmeyer-Gabbe, PhD, from Edanz (https://jp.edanz.com/ac) for editing the English text of a draft of this manuscript.

Appendix A. Supplementary data

Supplementary data to this article can be found online at https://doi.org/10.1016/j.jddst.2023.104981.

References

[1] S.K. Asrani, H. Devarbhavi, J. Eaton, P.S. Kamath, Burden of liver diseases in the world, J. Hepatol. 70 (2019) 151–171.
[2] F. Tacke, T. Luedde, C. Trautwein, Inflammatory pathways in liver homeostasis and liver injury, Clin. Rev. Allergy Immunol. 36 (2009) 4–12.
[3] M. Bilzer, F. Roggel, A.L. Gerbes, Role of Kupffer cells in host defense and liver disease, Liver Int. 26 (2006) 1175–1186.
[4] P. Li, K. He, J. Li, Z. Liu, J. Gong, The role of Kupffer cells in hepatic diseases, Mol. Immunol. 85 (2017) 222–229.
[5] P. Kleczkowska, D. Sulejczak, M. Zaremba, Advantages and disadvantages of disulfiram coadministered with popular addictive substances, Eur. J. Pharmacol. 904 (2021), 174143.
[6] J.L. Allensworth, M.K. Evans, F. Bertucci, A.J. Aldrich, R.A. Festa, P. Finetti, N. T. Ueno, R. Safi, D.P. McDonnell, D.J. Thiele, S. Van Laere, G.R. Devi, Disulfiram (DSF) acts as a copper ionophore to induce copper-dependent oxidative stress and mediate anti-tumor efficacy in inflammatory breast cancer, Mol. Oncol. 9 (2015) 1155–1168.
[7] E. Toda, A. Sawada, K. Takeuchi, K. Wakamatsu, A. Ishikawa, N. Kuwahara, Y. Sawa, S. Hatanaka, K. Kokubo, K. Makino, H. Takahashi, Y. Endo, S. Kunugi, M. Terasaki, Y. Terasaki, K. Matsushima, Y. Terashima, A. Shimazu, Inhibition of the chemokine signal regulator FROUNT by disulfiram ameliorates crescentic glomerulonephritis, Kidney Int. 102 (2022) 1276–1290.
[8] Y. Terashima, E. Toda, M. Itakura, M. Otsuji, S. Yoshinaga, K. Okumura, F.H. W. Shand, Y. Komohara, M. Takeda, K. Kokubo, M.C. Chen, S. Yokoi, H. Rokutan, Y. Kofuku, K. Ohnishi, M. Ohira, T. Iizasa, H. Nakano, T. Okabe, H. Kojima, A. Shimizu, S. Kanegasaki, M.R. Zhang, I. Shimada, H. Nagase, H. Terasawa, K. Matsushima, Targeting FROUNT with disulfiram suppresses macrophage accumulation and its tumor-promoting properties, Nat. Commun. 11 (2020) 609.
[9] P. Zhao, X. Tang, Y. Huang, Teaching new tricks to old dogs: a review of drug repositioning of disulfiram for cancer nanomedicine, VIEW 2 (2021), 20200127.
[10] M. Setshedi, J.R. Wands, S.M. de la Monte, Acetaldehyde adducts in alcoholic liver disease, Oxid. Med. Cell. Longev. 3 (2010) 178–185.
[11] J. Gueldner, C. Sayes, E. Abel, E. Bruce, Emerging associations of the ALDH2*2 polymorphism with disease susceptibility, J. Drug Metabol. Toxicol. 7 (2016), 1000202.
[12] Y.N. Zhang, W. Poon, A.J. Tavares, I.D. McGilvray, W.C.W. Chan, Nanoparticle-liver interactions: cellular uptake and hepatobiliary elimination, J. Contr. Release 240 (2016) 332–348.
[13] L. Shao, S. Shen, H. Liu, Recent advances in PLGA micro/nanoparticle delivery systems as novel therapeutic approach for drug-resistant tuberculosis, Front. Bioeng. Biotechnol. 10 (2022), 941077.
[14] Q. Chen, Y. Xue, J. Sun, Kupffer cell-mediated hepatic injury induced by silica nanoparticles in vitro and in vivo, Int. J. Nanomed. 8 (2013) 1129–1140.
[15] A. Boey, H.K. Ho, All roads lead to the liver: metal nanoparticles and their implications for liver health, Small 16 (2020), 2000153.
[16] H.K. Mandl, E. Quijano, H.W. Suh, E. Sparago, S. Oeck, M. Grun, P.M. Glazer, W. M. Saltzman, Optimizing biodegradable nanoparticle size for tissue-specific delivery, J. Contr. Release 314 (2019) 92–101.
[17] J. Li, C. Chen, T. Xia, Understanding nanomaterial-liver interactions to facilitate the development of safer nanoapplications, Adv. Mater. 34 (2022), 2106456.
[18] S.R. Popielarski, S.H. Lieskovan, S.W. French, T.J. Triche, M.E. Davis, A nanoparticle-based model delivery system to guide the rational design of gene delivery to the liver. 2. In vitro and in vivo uptake results, Bioconjugate Chem. 16 (2005) 1071–1080.
[19] A. Banerjee, L.O. Billey, W.L. Shelver, Uptake and toxicity of polystyrene micro/nanoplastics in gastric cells: effects of particle size and surface functionalization, PLoS One 16 (2021), e0260803.
[20] L.D.Q. Jiménez, R. Guzmán-Guillén, G.M. Cătunescu, A. Campos, V. Vasconcelos, Á. Jos, A.M. Cameán, A new method for the simultaneous determination of cyanotoxins (Microcystins and Cylindrospermopsin) in mussels using SPE-UPLC-MS/MS, Environ. Res. 185 (2020), 109284.
[21] Y. Yamanaka, T. Yamamoto, T. Egashira, Effects of cephem antibiotics on rat liver aldehyde dehydrogenases, Jpn. J. Pharmacol. 33 (1984) 717–723.
[22] B. Kokhanyuk, K. Bodo, G. Setalo Jr., P. Nemeth, P. Engelmann, Bacterial engulfment mechanism is strongly conserved in evolution between earthworm and human immune cells, Front. Immunol. 12 (2021), 733541.

[23] L. Palanikumar, S. Al-Hosani, M. Kalmouni, V.P. Nguyen, L. Ali, R. Pasricha, F. N. Barrera, M. Magzoub, pH-responsive high stability polymeric nanoparticles for targeted delivery of anticancer therapeutics, Commun. Biol. 3 (2020) 95.
[24] P. Marcianes, S. Negro, L.G. Garcia, C. Montejo, E. Barcia, A.F. Carballido, Surface-modified gatifloxacin nanoparticles with potential for treating central nervous system tuberculosis, Int. J. Nanomed. 12 (2017) 1959–1968.
[25] S. Patil, A. Sandberg, E. Heckert, W. Self, S. Seal, Protein adsorption and cellular uptake of cerium oxide nanoparticles as a function of zeta potential, Biomaterials 28 (2007) 4600–4607.
[26] L. Chen, J.M. Mccrate, J.C.M. Lee, H. Li, The role of surface charge on the uptake and biocompatibility of hydroxyapatite nanoparticles with osteoblast cells, Nanotechnology 22 (2011), 15708.
[27] Y. Xiao, W. Xu, Y. Komohara, Y. Fujiwara, H. Hirose, S. Futaki, T. Niidome, Effect of surface modifications on cellular uptake of gold nanorods in human primary cells and established cell lines, ACS Omega 5 (2020), 32744–32725.
[28] S.H. Cheng, F.C. Li, J.S. Souris, C.S. Yang, F.G. Tseng, H.S. Lee, C.T. Chen, C. Y. Dong, L.W. Lo, Visualizing dynamics of sub-hepatic distribution of nanoparticles using intravital multiphoton fluorescence microscopy, ACS Nano 6 (2012) 4122–4131.
[29] C. Wang, J. Yang, H. Han, J. Chen, Y. Wang, Q. Li, Y. Wang, Disulfiram-loaded porous PLGA microparticle for inhibiting the proliferation and migration of non-small-cell lung cancer, Int. J. Nanomed. 12 (2017) 827–837.
[30] H. Fasehee, A. Ghavamzadeh, K. Alimoghaddam, S.A. Ghaffari, S. Faghihi, A comparative cytotoxic evaluation of disulfiram encapsulated PLGA nanoparticles on MCF-7 Cells, Int. J. Hematol. Oncol. Stem Cell Res. 11 (2) (2017) 102–107.
[31] S.A. Abouelmagd, B. Sun, A.C. Chang, Y.J. Ku, Y. Yeo, Release kinetics study of poorly water-soluble drugs from nanoparticles: are we doing it right? Mol. Pharm. 12 (2015) 665–1004.
[32] I. Hassan, A.A. Khan, S. Aman, W. Qamar, H. Ebaid, J. Al-Tamimi, I.M. Alhazza, A. M. Rady, Restrained management of copper level enhances the antineoplastic activity of imatinib in vitro and in vivo, Sci. Rep. 8 (2018) 1682.
[33] M. Marselos, S.C. Strom, G. Michalopoulos, Effect of phenobarbital and 3-methyl-cholanthrene on aldehyde dehydrogenase activity in cultures of HepG2 cells and normal human hepatocytes, Chem. Biol. Interact. 62 (1987) 75–88.
[34] J.J. Lipsky, M.L. Shen, S. Naylor, Overview-In vitro inhibition of aldehyde dehydrogenase by disulfiram and metabolites, Chem. Biol. Interact. 130–132 (2001) 81–91.
[35] B. Jin-Smith, N. Jn-Simon, S. Basha, C. Sun, S. Wu, J.M. Barkin, L. Pi, Acetaldehyde dehydrogenases in liver zonation and liver cancer, Gene Expr. 22 (2023) 66–76.
[36] C. He, Y. Hu, L. Yin, C. Tang, C. Yin, Effects of particle size and surface charge on cellular uptake and biodistribution of polymeric nanoparticles, Biomaterials 31 (2010) 3657–3666.
[37] X. Cheng, X. Tian, A. Wu, J. Li, J. Tian, Y. Chong, Z. Chai, Y. Zhao, C. Chen, C. Ge, Protein corona influences cellular uptake of gold nanoparticles by phagocytic and nonphagocytic cells in a size-dependent manner, ACS Appl. Mater. Interfaces 7 (2015) 20568–20575.
[38] T.L. McGinnity, V. Sokolova, O. Prymak, P.D. Nallathamby, M. Epple, R.K. Roeder, Colloidal stability, cytotoxicity, and cellular uptake of HfO_2 nanoparticles, J. Biomed. Mater. Res. 109 (2021) 1407–1417.
[39] I.L. Hsiao, A.M. Gramatke, R. Joksimovic, M. Sokolowski, N. Gradzielski, A. Haase, Size and cell type dependent uptake of silica nanoparticles, J. Nanomed. Nanotechnol. 5 (2014), 1000248.
[40] M. Daigneault, J.A. Preston, H.M. Marriott, M.K.B. Whyte, D.H. Dockrell, The identification of markers of macrophage differentiation in PMA-stimulated THP-1 cells and monocyte-derived macrophages, PLoS One 5 (2010), e8668.
[41] V. Jaumouille, C.M. Waterman, Physical constraints and forces involved in phagocytosis, Front. Immunol. 11 (2020) 1097.
[42] N. Means, C.K. Elechalawar, W.R. Chen, R. Bhattacharya, Revealing micropinocytosis using nanoparticles, Mol. Aspect. Med. 83 (2022), 100993.
[43] M. Mettlen, P.H. Chen, S. Srinivasan, G. Danuser, S.L. Schmid, Regulation of clathrin-mediated endocytosis, Annu. Rev. Biochem. 87 (2018) 871–896.
[44] A.L. Kiss, E. Botos, Endocytosis via caveolae: alternative pathway with distinct cellular compartments to avoid lysosomal degradation? J. Cell Mol. Med. 13 (2009) 1228–1237.
[45] M.S. de Almeida, E. Susnik, B. Drasler, P. Taladriz-Blanco, A. Petri-Fink, B. Rothen-Rutishauser, Under standing nanoparticle endocytosis to improve targeting strategies in nanomedicine, Chem. Soc. Rev. 50 (2021) 5397–5434.
[46] G. Griffiths, J. Gruenberg, M. Marsh, J. Wohlmann, A.T. Jones, R.G. Parton, Nanoparticle entry into cells; the cell biology weak link, Adv. Drug Deliv. Rev. 188 (2022), 114403.
[47] J.V.V. Arafiles, H. Hirose, M. Akishiba, S. Tsuji, M. Imanishi, S. Futaki, Stimulating macropinocytosis for intracellular nucleic acid and protein delivery: a combined strategy with membrane-lytic peptides to facilitate endosomal escape, ACS Bioconjug. Chem. 31 (2020) 547–553.
[48] W. Guo, S. Chen, C. Li, J. Xu, L. Wang, Application of disulfiram and its metabolites in treatment of inflammatory disorders, Front. Pharmacol. 12 (2022), 795078.
[49] X. Huang, P. Sun, Y. Qin, X. Wang, M. Wang, Y. Lin, R. Zhou, W. Hu, Q. Liu, X. Yu, A. Qin, Disulfiram attenuates MCMV-induced pneumonia by inhibition of NF-κB/NLRP3 signaling pathway in immunocompromised mice, Int. Immunopharm. 103 (2022), 108453.
[50] J.K. Park, T. Utsumi, Y.E. Seo, Y. Deng, A. Satoh, W.M. Saltzman, Y. Iwakiri, Cellular distribution of injected PLGA-nanoparticles in the liver, Nanomedicine 12 (2016) 1365–1374.
[51] H. Wang, C.A. Thorling, X. Liang, K.R. Bridle, J.E. Grice, Y. Zhu, D.H.G. Crawford, Z.P. Xu, X. Liu, M.S. Roberts, Diagnostic imaging and therapeutic application of nanoparticles targeting the liver, J. Mater. Chem. B 3 (2015) 939.
[52] F. Danhier, E. Ansorena, J.M. Silv, R. Coco, A.L. Breton, V. Preat, PLGA-based nanoparticles: an overview of biomedical applications, J. Contr. Release 161 (2012) 505–522.
[53] S. Ghosh, A. Sarkar, S. Bhatacharyya, P.C. Sil, Silymarin protects mouse liver and kidney from thioacetamide induced toxicity by scavenging reactive oxygen species and activating PI3K-Akt pathway, Front. Pharmacol. 7 (2016) 481.
[54] X. Dong, J. Liu, Y. Xu, H. Cao, Role of macrophages in experimental liver injury and repair in mice, Exp. Ther. Med. 17 (2019) 3835–3847, submitted for publication.
[55] X. Wu, N. Hollingshead, J. Roberto, A. Kenerson, A. Chen, I. Strickland, H. Horton, R. Yeung, R. Soysa, I.N. Crispe, Human liver macrophage subsets defined by CD32, Front. Immunol. 11 (2020) 2108.
[56] J. Zhao, H. Wang, J. Zhang, F. Ou, J. Wang, T. Liu, J. Wu, Disulfiram alleviates acute lung injury and related intestinal mucosal barrier impairment by targeting GSDMD-dependent pyroptosis, J. Inflamm. 19 (2022) 17.
[57] A. Ou, J. Zhang, Y. Fang, R. Wang, X. Tang, P. Zhao, Y. Zhao, M. Zhang, Y. Huang, Disulfiram-loaded lactoferrin nanoparticles for treating inflammatory diseases, Acta Pharmacol. Sin. 42 (2021) 1913–1920.
[58] W. Ngo, S. Ahmed, C. Blackadar, B. Bussin, Q. Ji, S.M. Mladjenovic, Z. Sepahi, W.C. W. Chan, Why nanoparticles prepfer liver macrophage cell uptake in *vivo*, Adv. Drug. Deliv. 185 (2022), 114238.
[59] V. Kannappan, M. Ali, B. Small, G. Rajendran, S. Elzhenni, H. Taj, W. Wang, Q. P. Dou, Recent advances in repurposing disulfiram and disulfiram derivatives as copper-dependent anticancer agents, Front. Mol. Biosci. 8 (2021), 741316.
[60] E. Swider, S. Maharjan, K. Houkes, N.K. van Riessen, C. Figdor, M. Srinivas, O. Tagit, Forster resonance energy transfer-based stability assessment of PLGA nanoparticles in vitro and in vivo, ACS Appl. Bio Mater. 2 (2019) 1131–1140.
[61] X.M. Yang, Z. Wu, X.Q. Wang, Y.Q. Zhou, L. Zhu, D.X. Li, H.Z. Nie, Y.H. Wang, J. Li, X.Y. Ma, Disulfiram inhibits liver fibrosis in rats by suppressing hepatic stellate cell activation and viability, BMC Pharmacol. Tox. 23 (2022) 54.
[62] P. Chen, Y.K. Zhou, C.S. Han, L.J. Chen, Y.M. Wang, Z.M. Zhuang, S. Lin, Y. H. Zhou, J.H. Jiang, Stem cells from human exfoliated deciduous teeth alleviate liver cirrhosis via inhibition of Gasdermin D-executed hepatocyte pyroptosis, Front. Immunol. 13 (2022), 860225.
[63] L. Ramer, M. Tihy, N. Goossens, J.L. Frossard, L.R. Brandt, L. Spahr, Disulfiram-induced acute liver injury, Case Reports Hepatol 2020 (2020), 8835647.